coatings

MDPI

Article

Performance Analysis of the Self-Pumping Hydrodynamic Mechanical Seal with a Conical Convergent Diffuser Groove

Xuchen Su, Jianjun Sun *, Chenbo Ma and Qiuping Yu

Department of Mechanical and Electrical Engineering, Nanjing Forestry University, Nanjing 210037, China; suxuchen@njfu.edu.cn (X.S.); machenbo@njfu.edu.cn (C.M.); yuqiuping03@njfu.edu.cn (Q.Y.)
* Correspondence: sunjianjun@njfu.edu.cn; Tel.: +86-139-1335-0626

Abstract: Requirements such as high opening force, low leakage rate, and design without matching auxiliary flushing systems are expected of the modern fluid machinery shaft seals used in the process industry. A self-pumping hydrodynamic mechanical seal with a conical convergent diffuser groove is proposed and its sealing performance is studied by numerical simulation in this paper. Further, its sealing performance is compared to that of a flat-bottomed equal cross-sectional diffuser groove and the results have shown that the proposed seal has more superior sealing performance. The influence of structural and operating parameters on the sealing performance of the proposed seal is discussed and its working mechanism is explained. The results have shown that when the structural parameters of the spiral groove and the operating parameters are the same, the proposed design has a similar leakage rate and a higher opening force. The conical convergent diffuser groove has better wrapping properties, whereas the fluid energy is utilized more efficiently, improving the sealing interface opening force. The taper degree variation causes a slight change to the pressure at the root of the spiral groove, causing slight fluctuations in the seal leakage rate. The research results broaden the design of non-contact mechanical seals and provide a theoretical basis for the engineering application of the proposed self-pumping hydrodynamic mechanical seal with a conical convergent diffuser groove.

Keywords: mechanical seal; conical convergent diffuser groove; sealing performances; CFD

check for updates

Citation: Su, X.; Sun, J.; Ma, C.; Yu, Q. Performance Analysis of the Self-Pumping Hydrodynamic Mechanical Seal with a Conical Convergent Diffuser Groove. *Coatings* **2022**, *12*, 1058. https://doi.org/10.3390/coatings12081058

Academic Editors: Rahmat Ellahi and Eduardo Guzmán

Received: 6 June 2022
Accepted: 25 July 2022
Published: 26 July 2022

Publisher's Note: MDPI stays neutral with regard to jurisdictional claims in published maps and institutional affiliations.

Copyright: © 2022 by the authors. Licensee MDPI, Basel, Switzerland. This article is an open access article distributed under the terms and conditions of the Creative Commons Attribution (CC BY) license (https://creativecommons.org/licenses/by/4.0/).

1. Introduction

Nowadays, dry gas and upstream pumping mechanical seals based on hydrodynamic and hydrostatic pressure effects are commonly used as the rotary shaft seals in petrochemical, nuclear power, and aviation fields, among others [1–3]. This type of non-contact mechanical seal includes a complete fluid film between the rotating ring and the stationary ring end faces during the operation, avoiding the wear caused by the hard solid-phase contact and achieving a controllable leakage rate, thus drawing people's attention [4]. In recent years, researchers focused mainly on the optimization of surface parameters and sealing performance [5–7], the simulation of flow fields between seal end faces [8,9], and fluid-structure interaction and thermal-mechanical coupling effects [10]. However, to maintain the sealing interface fluid film stability, it is often necessary to build a matching auxiliary flushing system for both the dry gas seals and upstream pumping mechanical seals [11], which increases the initial investment and operational costs. Moreover, in this type of non-contact mechanical seal, the fluid wedges between seal rings to form dynamic pressure by opening grooves on the sealing end face. This separates the rotating and stationary rings, increasing the seal service life; however, there is also a risk that the solid particles in the wedge-in fluid will climb over the sealing dam and destroy the seal end face [12,13].

To solve the problem, Sun et al. [14–16] invented a fluid pump-out non-contact mechanical seal with spiral grooves on the rotating ring end face. Unlike the traditional

non-contact mechanical seal, this seal forms the opening force to separate the rotating and stationary ring. The fluid flowing out of the deflector hole (or annular groove) at the sealing dam is pressurized and accelerated by the spiral groove. The relative decrease in velocity increases the pressure of the fluid within the spiral groove as the cross-sectional area of the spiral groove increases. Since the fluid flows away from the sealing dam, potential solid particles in the fluid will not damage the seal end face. Further, Gu et al. [17] analyzed this pump-out mechanical seal using the orthogonal test and detected significant factors affecting its sealing performance; the preliminary optimized seal structure was proposed. Chen et al. [18] applied the Discrete Phase Model (DPM) method in Fluent to assess whether the self-pumping hydrodynamic and hydrostatic mechanical seal has a better chip removal rate for different particle diameters and particle volume concentrations compared to traditional non-contact mechanical seals. In a single-factor performance analysis of the self-pumping mechanical seal, Sun et al. [19] found that the sealing interface opening force decreases as the rotating speed increases, which practically makes it unapplicable in extreme operating conditions. For this reason, Ge et al. [20] constructed a diffuser self-pumping hydrodynamic and hydrostatic mechanical seal with a diffuser groove located on the outer rotating ring edge. The design was based on the working principle of the diffuser of centrifugal pump and centrifugal compressor. By comparing and analyzing the sealing performance of the diffuser self-pumping mechanical seal to the ordinary self-pumping mechanical seal, it was found that the diffuser groove can effectively increase the opening force with the rotating speed. However, the diffuser groove width limits its diffusing effect.

For dry gas and upstream pumping mechanical seals, they need a matching auxiliary flushing system to reduce the friction heat of the sealing interface so that the liquid film between the seal rings is stable. However, the matching auxiliary flushing system increases the complexity of the mechanical seal sealing structure and the cost of operation and maintenance. Hence, a self-pumping hydrodynamic and hydrostatic mechanical seal that does not require an auxiliary flushing system is invented to simplify the seal structure and has good sealing performances. However, in subsequent studies, it was found that its sealing interface opening force decreases as the rotating speed increases making it difficult for non-contact functioning under extreme conditions. Therefore, there is a requirement to propose a non-contact mechanical seal that does not require a matching auxiliary flushing system and whose opening force of the seal end face increases with the rotating speed.

In this paper, a self-pumping hydrodynamic mechanical seal with a conical convergent diffuser groove (CCDG) is proposed. The design of CCDG is based on the working principle of a diffusor in centrifugal compressors or pump and incorporates the hydraulic effect of convergent clearance. The sealing performance of the self-pumping hydrodynamic mechanical seal with a CCDG and a flat-bottomed equal cross-sectional diffuser groove (FEDG) is compared. The study is carried out by utilizing the Fluent numerical simulation. The influences of structural and operating parameters on the sealing performance of the proposed seal are investigated. The working mechanism behind its high hydrodynamic pressure and low leakage rate is explained, providing the theoretical basis for further engineering applications.

2. The Rotating and Stationary Ring Structure

Figure 1 shows the structure of the rotating and stationary ring of the self-pumping hydrodynamic mechanical seals with a diffuser groove. As illustrated in Figure 1a, it consists of a sealing dam, backward curved spiral grooves, sealing weirs, and a diffuser groove (located on the rotating ring end face). The annular groove and deflector holes are set on the stationary ring end face (Figure 1b).

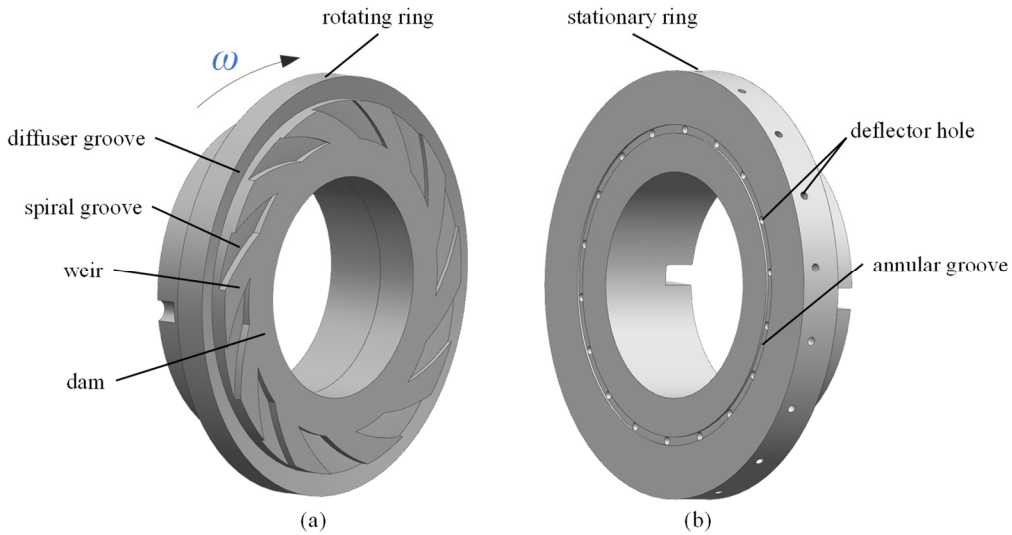


Figure 1. Structure of the rotating and stationary rings of the diffuser groove self-pumping hydrodynamic mechanical seal: (**a**) The rotating ring; (**b**) The stationary ring. The arrow on the image indicates the direction of rotation of the rotating ring.

Figure 2a illustrates the structure of seal rings with an FEDG; the diffuser groove depth is constant along the radial direction (moving from the inlet to the outlet). Further, Figure 2b shows the structure of both the rotating and stationary rings with a CCDG designed by the authors. The circumferential cross-sectional area of the diffuser groove decreases radially from the inlet to the outlet and has a convergent conic shape in the fluid flow direction. The fluid flow direction in the sealing interface is indicated by the arrow (see Figure 2). The diffuser groove inlet depth is equal to the spiral groove depth to ensure a smooth flow path. The variable λ is introduced to characterize the diffuser groove taper degree (when $\lambda = 0$, the diffuser groove is the FEDG):

$$\lambda = 1 - \frac{h_{\mathrm{ko}}}{h_{\mathrm{ki}}}, \tag{1}$$

where h_{ko} is the diffuser groove outlet depth and h_{ki} is its inlet depth.

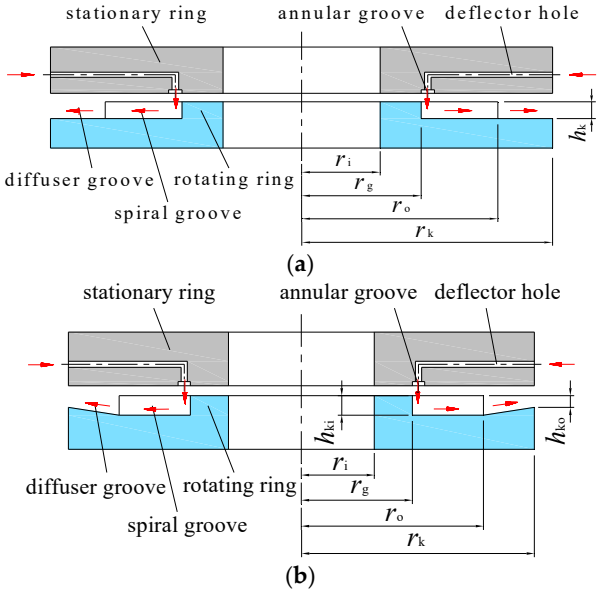


Figure 2. The diffuser groove structure: (**a**) The flat-bottomed equal cross-sectional diffuser groove; (**b**) The conical convergent diffuser groove.

The spiral groove is a logarithmic spiral groove and its polar coordinate expression is defined as follows:

$$r = r_g e^{\theta} \tan \alpha, \quad (2)$$

where r_g is the root radius of the spiral groove, θ is the rotation angle, and α is the helix angle.

3. Numerical Simulation Analysis

3.1. Basic Assumptions

The calculation of the end-face flow field of the hydrodynamic mechanical seal is relatively complicated. In reciprocating hydraulic systems, the lubricating film thickness h must be determined mainly by the shear flow rather than the pressure flow [21]. However, in rotary shaft seals, the film thickness is mainly determined by pressure flow. Thus, to simplify, the following assumptions are made based on the model studied in this work [22]. Those include:

1. The fluid medium is a Newtonian fluid and is a continuous medium.
2. The fluid flow between the sealing interface is a steady laminar flow with constant temperature and viscosity.
3. The sealing face is perfectly smooth; the effect of roughness on fluid flow was ignored.
4. The liquid film is very thin; pressure and density changes in the thickness direction are ignored.
5. The temperature of the sealing rings and the material's mechanical properties do not change with time.
6. There is no relative slippage between the fluid medium and the sealing interface.
7. The system disturbance and vibration during the working process are not considered.

3.2. The Computational Region Model

Considering the high symmetry of seal ring structures and the flow field of the sealing interface in the proposed mechanical seal with a CCDG, the fluid flow state in each groove is the same. To reduce the calculation cost, the groove number is denoted as N_g, and the $1/N_g$ segment of the whole flow field [23] is taken as the computational region. That is, a groove and the connected sealing dam region are used as the computational model, indicated as the zone ABCD in Figure 3.

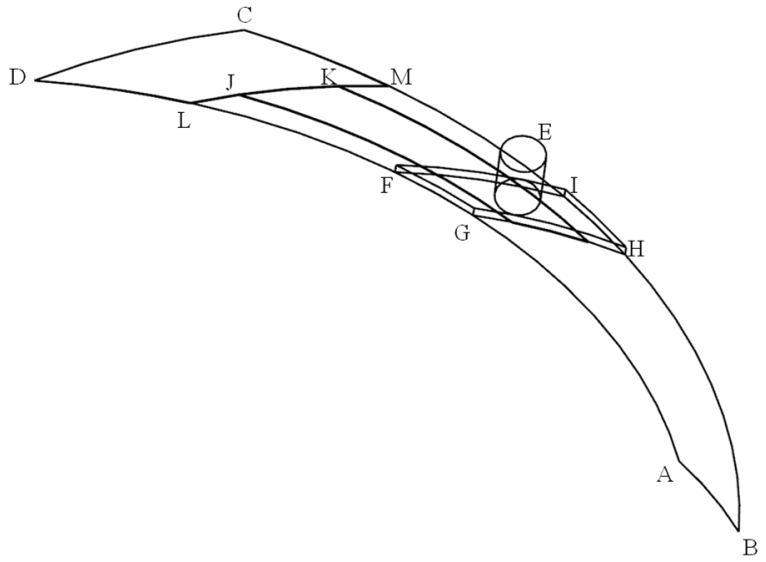


Figure 3. Computational region of the flow.

3.3. The Governing Equation

Based on the above basic assumptions and geometric model, the fluid flow between the sealing interfaces is defined as a steady flow and satisfies the simplified N-S equation [24]. The simplified N-S equation in the x-direction is written as:

$$\rho\left(u\frac{\partial u}{\partial x}+v\frac{\partial u}{\partial y}\right)=-\frac{\partial p}{\partial x}+\mu\left(\frac{\partial^2 u}{\partial x^2}+\frac{\partial^2 u}{\partial y^2}\right) \tag{3}$$

The simplified N-S equation in the y-direction is written as:

$$\rho\left(u\frac{\partial v}{\partial x}+v\frac{\partial v}{\partial y}\right)=-\frac{\partial p}{\partial y}+\mu\left(\frac{\partial^2 v}{\partial x^2}+\frac{\partial^2 v}{\partial y^2}\right) \tag{4}$$

where x and y are coordinate vectors, u and v are velocities along the x and y directions, respectively, ρ is the sealing medium density, μ is the sealing medium viscosity, and p is the sealing medium pressure.

The continuity equation is:

$$\frac{\partial u}{\partial x}+\frac{\partial v}{\partial y}=0 \tag{5}$$

Equations (3)–(5) are governing equations for solving the flow field of the sealing interface based on the N-S equation.

3.4. Boundary Conditions and Solver Settings

Given that Reynolds boundary conditions are close to the actual liquid film distribution and are adopted in the numerical analysis, they are used to define the boundary conditions of the computational region [25,26]. The specific settings are in Table 1.

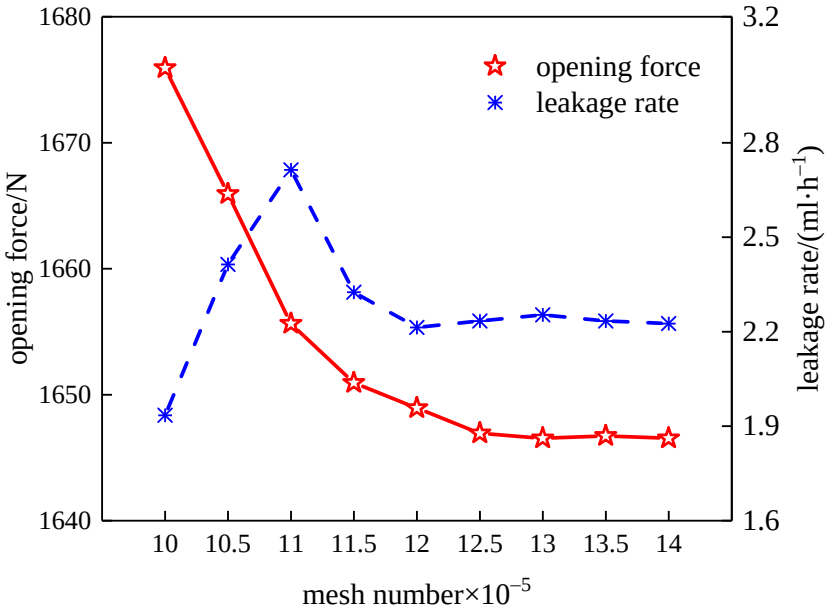
Table 1. Boundary condition settings.

Boundary Conditions	Boundary Type and Values
Deflector hole, *E*	pressure-inlet ($P \mid E = p_o$), p_o = 0.1–0.9 MPa
Inner diameter, *AB*	pressure-outlet ($P \mid AB = p_i$), $p_I = 0$
Outer diameter, *CD*	pressure-outlet ($P \mid CD = p_o$), p_o = 0.1–0.9 MPa
Annular groove, *FG*, *HI*	periodic boundary ($P \mid FG = P \mid HI$)
Liquid film, *AD*, *BC*	periodic boundary ($P \mid AD = P \mid BC$)
Bottom surface of deflector hole and upper surface of annular groove	interface
Bottom surface of annular groove and upper surface of liquid film	interface
Bottom surface of liquid film and upper surface of spiral groove	interface
Spiral groove outlet, *JK* and diffuser ring inner diameter side, *LM*	interface
Bottom surface of spiral groove	moving wall
Both sides and inner diameter side of spiral groove	moving wall
The rest of the walls	stationary wall

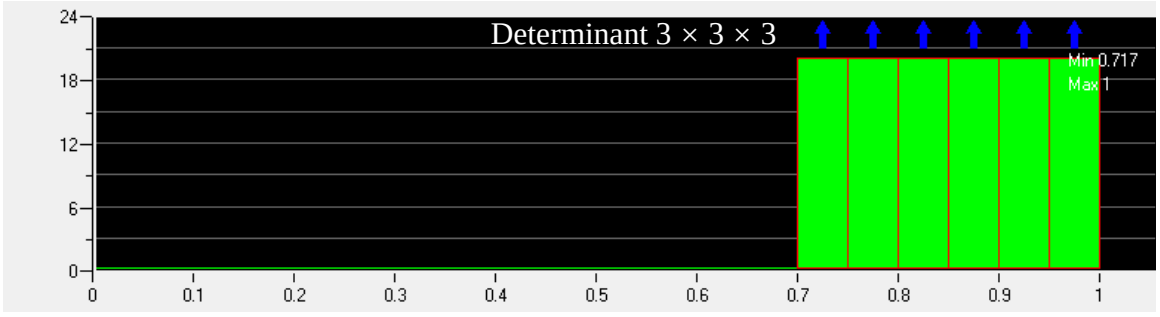
Since the governing Equations (3)–(5) are nonlinear partial differential equations, they cannot be solved analytically; therefore, the computational fluid dynamics (CFD) is used to solve the flow filed [27]. The selected solver parameters are listed as follows: three-dimensional double-precision solver, non-viscous fluid, steady-state laminar flow, "SIMPLEC" algorithm for pressure-velocity coupled computation, central differencing, and second upwind schemes for the discretization of diffusion and convective terms, respectively, and absolute convergence accuracy is 10^{-6}. "SIMPLEC" algorithm is an abbreviation for SIMPLE consistent, meaning coordinated "SIMPLE" algorithm (Semi-Implicit Method for Pressure Linked Equations).

3.5. Meshing Generation

The hexahedral structural mesh in the ICEM module is used to divide the computational region. Since the film thickness is on the micrometer scale and thus several orders of magnitude lower compared to other dimensions, the number of nodes on the model boundary is adopted to ensure the overall mesh quality, ensuring the high calculation accuracy [28]. As shown in Figure 4a, the grid independence is verified to determine the number of computational grids. The effects of mesh quality, calculation cost, and calculation accuracy are comprehensively considered; when the number of meshes in the computational domain increases to 1.27 million, the obtained opening force and leakage rate results remained unchanged. The mesh quality is checked by the quality inspection tool in ICEM, as illustrated in Figure 4b. The number indicating the mesh quality is above 0.7, and 97.024% of the meshes are in the interval of 0.95 to 1. The mesh is of high quality and can be used for calculation.



(**a**)



(**b**)

Figure 4. Meshing generation check: (**a**) grid independence verification; (**b**) mesh quality histogram.

4. Results and Discussion

The structural and operating parameters of the diffuser groove self-pumping hydrodynamic pressure mechanical seals used in the calculation are provided in Table 2.

Table 2. Boundary condition parameters.

Parameters	Value
Outer radius of the sealing ring r_k/mm	32.5~35
Outer radius of the spiral groove r_o/mm	30.6
Sealing medium	Water
Root radius of the spiral groove r_g/mm	23.875
Inner radius of the sealing ring r_i/mm	15.875
Spiral groove depth (diffuser groove inlet depth) $h_g = h_{ki}$, /μm	30~60
Film thickness h_c/μm	3
Width ratio of groove to diffuser groove γ	0.4–0.9
Groove number N_g	22~34
Helix angle α/(°)	22~50
Annular groove width L/mm	2
Annular groove depth H/mm	0.5
Diameter of deflector hole, D/mm	2
Differential pressure of the sealing medium Δp/MPa	0.1~0.9
Rotating speed n/r·min^{-1}	500~10,000

4.1. The Calculation Method Verification

The accuracy of the applied Fluent calculation method is verified in the previous study (reference [20]). As shown in Figure 5, the results have shown that the algorithm can calculate the flow field of the diffuser self-pumping hydrodynamic mechanical seal more accurately.

4.2. Comparative Analysis of Sealing Performances

4.2.1. The Opening Force and Leakage Rate

Figure 6 illustrates the influence of rotating speed variation on the sealing performance of self-pumping hydrodynamic mechanical seals with two different diffuser grooves. For the proposed seal, the fluid flowing through the spiral groove has higher kinetic energy as the rotating speed increases. When the fluid with higher kinetic energy enters the FEDG, its velocity decreases due to the increase in the cross-sectional area of the flow path. The part of kinetic energy is converted into pressure energy, increasing the opening force. When the rotating speed increases to a critical value (6000 r·min^{-1}), due to limited diffuser groove width, the high-speed fluid is pumped out of the diffuser groove into the sealing chamber. This is done without sufficiently converting the kinetic energy into pressure energy, decreasing the opening force. The existence of the CCDG builds an enclosed cavity; thus, the high-speed fluid accelerated by the spiral grooves can fully decelerate and convert its kinetic energy into pressure energy. With the increase in rotating speed, the spiral groove pumping capacity grows and the fluid pressure at the root of the spiral groove decreases. This decreases the pressure difference on both sides of the sealing dam, reducing the leakage rate of the sealing interface. Although the opening forces of the self-pumping hydrodynamic mechanical seals with two different diffuser grooves are not similar, the fluid pressure at the outer diameter side of the sealing dam is almost the same. Hence, both structures have rather similar leakage rates.

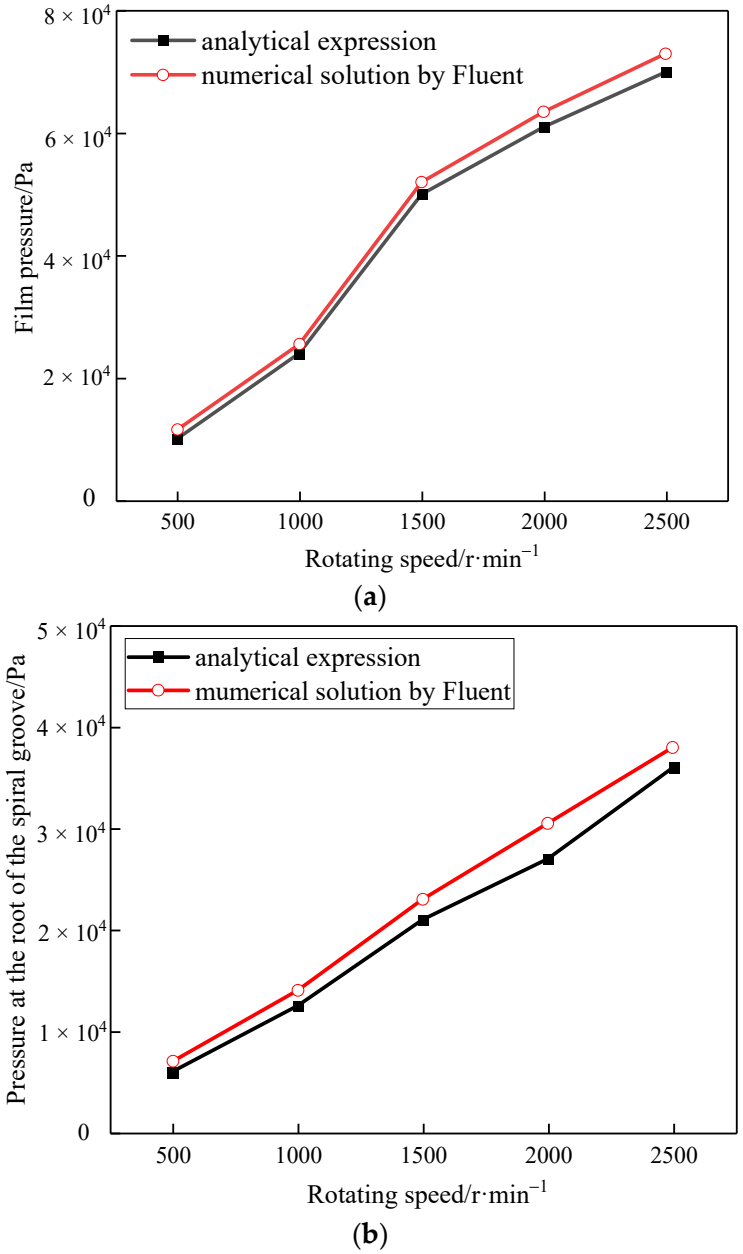


Figure 5. The verification of the calculation method: (**a**) The spiral groove verification; (**b**) The diffuser groove verification.

4.2.2. Film Pressure Distribution

The liquid film pressure cloud chart at the sealing interface of seals with an FEDG and a CCDG during the steady-state operation is shown in Figure 7. Compared to the self-pumping hydrodynamic mechanical seal with an FEDG, the seal with a CCDG benefits from the setting of CCDG. It provides a relatively stable pressurization zone which ensures that the high-pressure fluid will not rapidly flow out and dilute. This results in a higher pressure-peak and a larger high-pressure fluid area at the sealing interface, effectively increasing the opening force at the sealing interface. The pumping-out of the fluid reduces the pressure at the root of the spiral groove and decreases the medium pressure difference on both sides of the sealing dam. Such behavior explains the low leakage rate of the self-pumping hydrodynamic mechanical seals with different diffuser grooves.

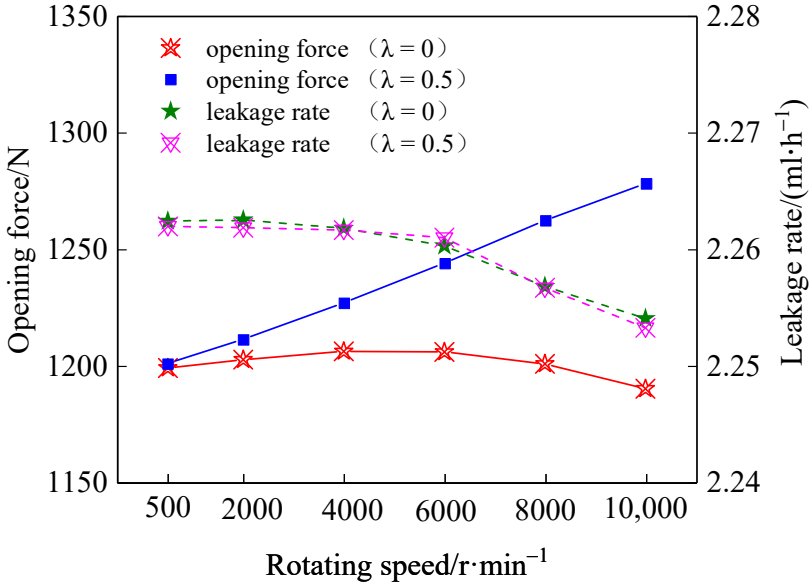


Figure 6. Characteristic performance curve of the diffuser self-pumping mechanical seal. (r_k = 34 mm, h_{ki} = h_g = 50 μm, r_o = 30.6 mm, N_g = 32, γ = 0.5, α = 30°, Δp = 0.5 MPa).

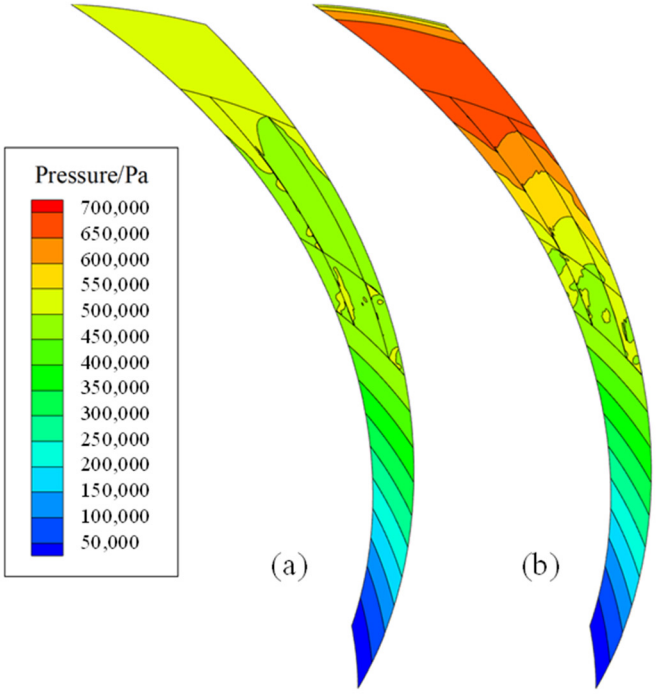


Figure 7. Film pressure distribution of self-pumping hydrodynamic mechanical seals with different diffuser grooves: (**a**) The self-pumping hydrodynamic mechanical seal with an FEDG: (r_k = 34 mm, h_{ki} = h_g = 50 μm, r_o = 30.6 mm, N_g = 32, γ = 0.5, λ = 0, α = 30°, Δp = 0.5 MPa, n = 6000 r·min^{-1}); (**b**) The self-pumping hydrodynamic mechanical seal with a CCDG: (r_k = 34 mm, h_{ki} = h_g = 50 μm, r_o = 30.6 mm, N_g = 32, γ = 0.5, λ = 0.9, α = 30°, Δp = 0.5 MPa, n = 6000 r·min^{-1}).

4.3. Influence of Structural Parameters on the Sealing Performance

4.3.1. Influence of the Diffuser Groove Length

Figure 8a,b shows the influence of the diffuser groove length on the opening force and leakage rate of the sealing interface, respectively. With the increase in the outer diameter of the rotating ring, the capability of the sealing interface to carry the fluid increases and improves the opening force. Simultaneously, the increase in the diffuser groove space both

decelerates and pressurizes the high-speed fluid, fully converting its kinetic energy into pressure energy. The opening force of the sealing interface increases almost linearly, as shown in Figure 8a. When the rotating speed of the seal increases, the fluid flowing through the spiral groove gains more kinetic energy. The increasing diffuser groove length can thus effectively convert more kinetic energy of the fluid in the diffuser cavity into pressure energy, significantly increasing the opening force of the sealing interface opening force.

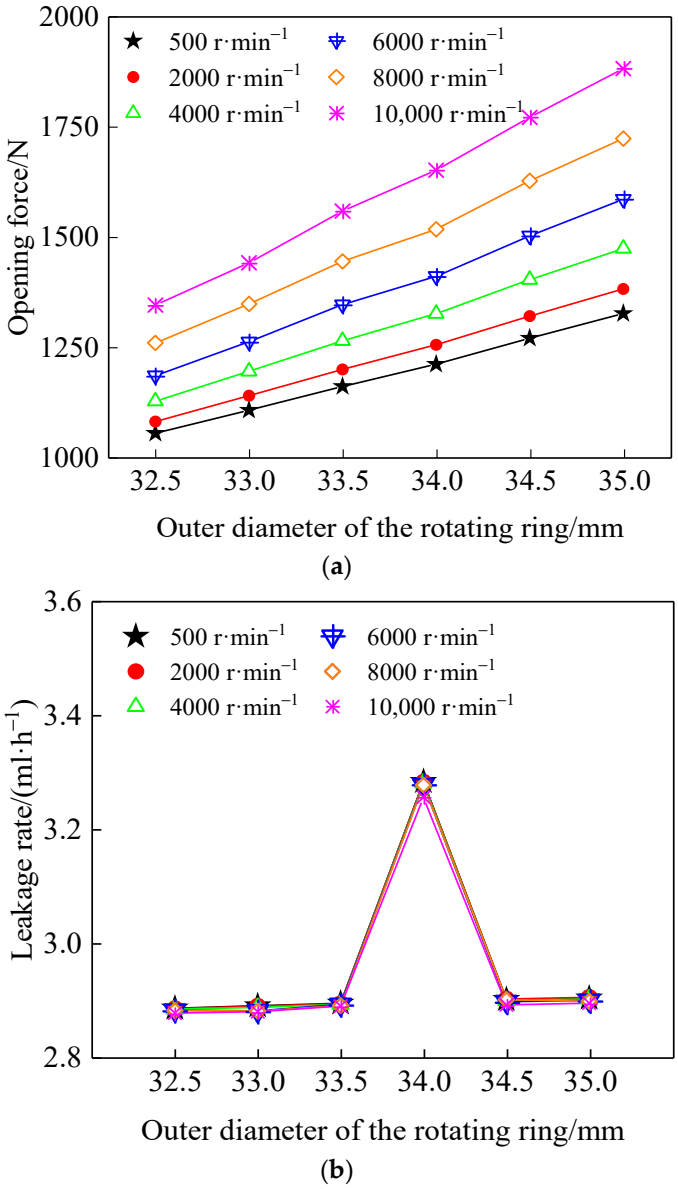


Figure 8. Influence of the diffuser groove length on its sealing performance: (**a**) Influence on the opening force; (**b**) Influence on the leakage rate. (h_ki = h_g = 50 μm, r_o = 30.6 mm, N_g = 22, γ = 0.5, λ = 0.9, $\alpha = 30°$, Δp = 0.5 MPa).

Figure 8b shows the influence of the diffuser groove length on the leakage rate. Given that the spiral groove length remains unchanged, increasing the diffuser groove length will make the fluid decelerate and diffuse more effectively. The peak fluid pressure in the diffuser groove will increase, gradually making it harder to pump the fluid and slowly increasing the pressure at the root of the spiral groove. Additionally, the medium pressure difference on both sealing dam sides will also increase, increasing the leakage rate. When the outer radius of the diffuser groove is r_k = 34 mm, the medium pressure difference on both sides of the sealing dam will reach the maximum value, resulting in the highest

leakage rate. As the diffuser groove length continues to increase, the excess groove volume will decrease the pressure at the root of the spiral groove. This will result in a state of small diffuser groove length (as described above), slowly increasing the leakage rate.

4.3.2. Influence of the Diffuser Groove Taper Degree

Figure 9a,b shows the influence of the diffuser groove taper degree on the sealing interface opening force and leakage rate, respectively. As the taper degree increases, the encapsulation of the diffuser groove improves, increasing its ability to gather fluid energy, resulting in a higher opening force. The increase in the rotating speed increases the fluid velocity; hence, more energy will be accumulated by the fluid in the diffuser chamber. Thus, the opening force formed by the fluid deceleration and diffusion will be higher.

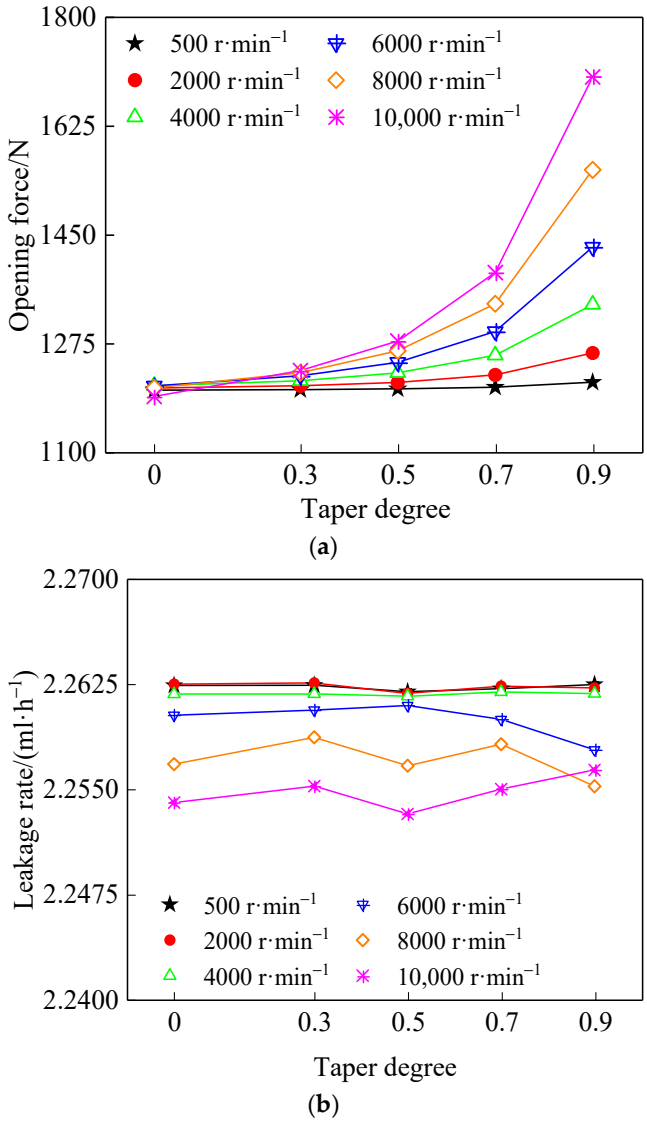


Figure 9. Influence of the diffuser groove taper degree on its sealing performance: (**a**) Influence on the opening force; (**b**) Influence on the leakage rate. (r_k = 34 mm, h_{ki} = h_g = 50 μm, r_o = 30.6 mm, N_g = 32, γ = 0.5, α = 30°, Δp = 0.5 MPa).

The taper degree variation causes a slight change in the pressure at the root of the spiral groove, causing fluctuations in the pressure difference on both sides of the sealing dam, resulting in the seal leakage rate fluctuations. When the taper degree remains the same, the increased rotating speed causes an increase in the fluid flow and a decrease in

the pressure at the root of the spiral groove. This reduces the pressure difference on both sides of the sealing dam and the leakage rate.

4.3.3. Influence of the Diffuser Groove Inlet Depth

To prevent the fluid flow from forming a step streamline at the axial section, only the case where the diffuser groove inlet depth (h_{ki}) is equal to the spiral groove depth (h_g) is discussed here. This was done to ensure that the basic assumptions provided in Section 3.1 will be satisfied. While keeping the other parameters constant, the variation in the spiral groove depth h_g will imply that the encapsulation of the diffuser cavity is changed. Figure 10a shows that the encapsulation of the diffuser cavity worsens with the increase in the diffuser groove inlet depth. The high-speed fluids overflow the diffuser cavity without sufficient deceleration and pressurization, as illustrated in Figure 11. The high-pressure peak and the high-pressure area of the fluid gradually decrease, reducing the sealing interface opening force. With the increase in rotating speed, the fluid flow rate that overflows the diffuser cavity without sufficient deceleration and pressurization will increase, increasing the opening force speed reduction.

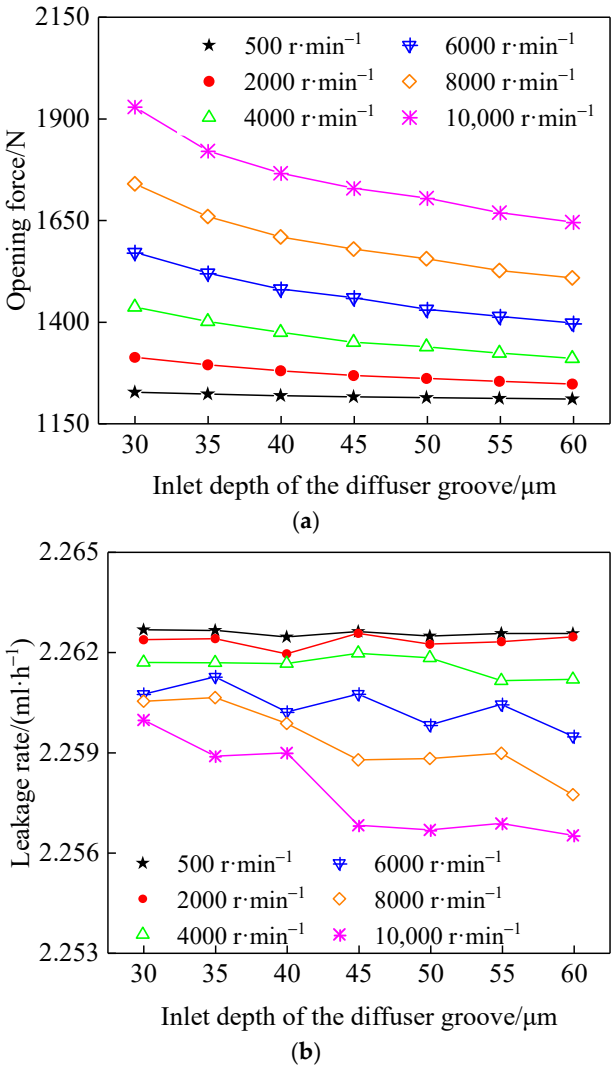


Figure 10. Influence of the diffuser groove inlet depth on its sealing performance: (**a**) Influence on the opening force; (**b**) Influence on the leakage rate. (r_k = 34 mm, r_o = 30.6 mm, N_g = 32, γ = 0.5, λ = 0.9, α = 30°, Δp = 0.5 MPa).

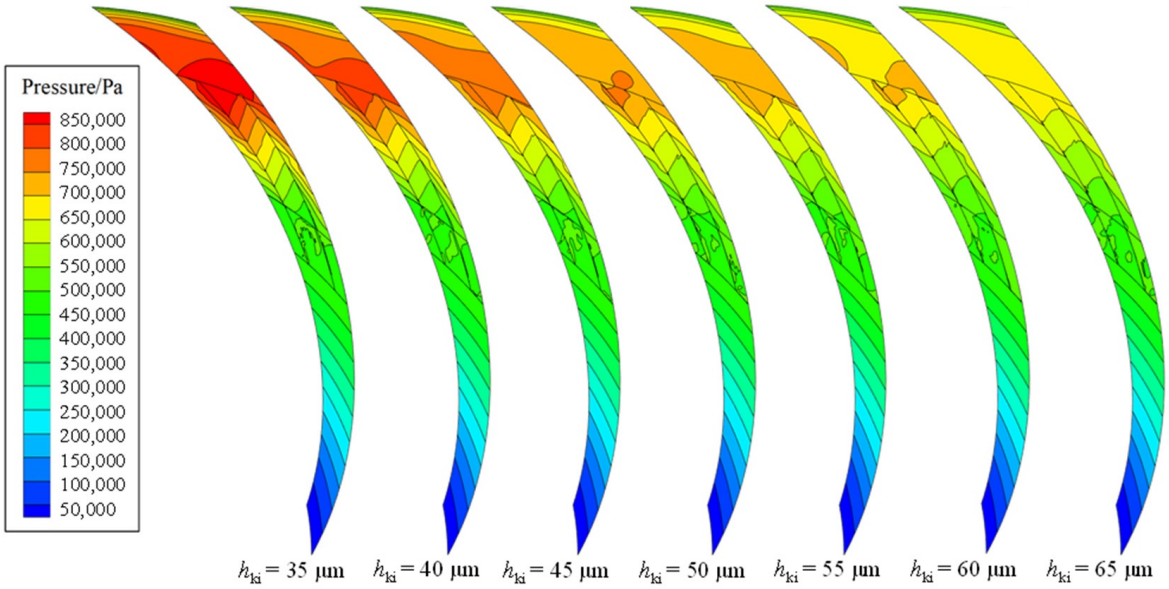


Figure 11. Film pressure cloud chart of the diffuser groove with different depths. (r_k = 34 mm, r_o = 30.6 mm, N_g = 32, γ = 0.5, λ = 0.9, α = 30°, Δp = 0.5 MPa, n = 6000·r·min^{-1}).

As shown in Figure 10b, at a low rotating speed, the spiral groove does less work on the fluid within the spiral groove, yielding a small, pumped fluid volume. The pressure at the root of the spiral groove is high, resulting in a high pressure difference on both sides of the sealing dam and causing a higher leakage rate. For the diffuser groove which has a constant taper degree and whose inlet depth increases with the spiral groove depth, the wrapping property of the diffuser chamber worsens, resulting in the pressure at the root of the spiral groove that is not very low, yielding a higher leakage rate. With the increase in the rotating speed, the flow rate of pumped fluid increases and the pressure at the root of the spiral groove decreases. Hence, the pressure difference on both sides of the sealing dam decreases, lowering the leakage rate. The increase in the spiral groove depth and the pumped fluid flow will further reduce the pressure at the root of the spiral groove, significantly reducing the leakage rate of the sealing interface.

4.3.4. Influence of the Width Ratio of Spiral Groove to the Diffuser Groove

To assess the influence of the relationship between the spiral groove outlet width and the single-period diffuser groove inlet width on the sealing performance, the width ratio of the spiral groove to the diffuser groove is defined as $\gamma = \widehat{JK}/\widehat{LM}$. The $\widehat{JK}$ is the spiral groove outlet width in the computational region (shown in Figure 3) and $\widehat{LM}$ is the single-period diffuser groove inlet width. As shown in Figure 12a, with the increase in the ratio, the opening force remains practically constant; however, its fluctuation becomes obvious at high rotating speed. The increase in the ratio implies that the spiral groove width increases while the outer radius remains constant. The width of the corresponding diffuser groove decreases and the distance of the fluid flowing through the working surface of the spiral groove increases, resulting in higher kinetic energy and dynamic pressure. However, when shortening the diffuser groove width, only part of the fluid kinetic energy will be converted into pressure energy. The remaining fluid overflows the diffuser cavity before the conversion into pressure energy; therefore, the area occupied by the peak pressure in the diffuser groove is not large, slightly increasing the opening force.

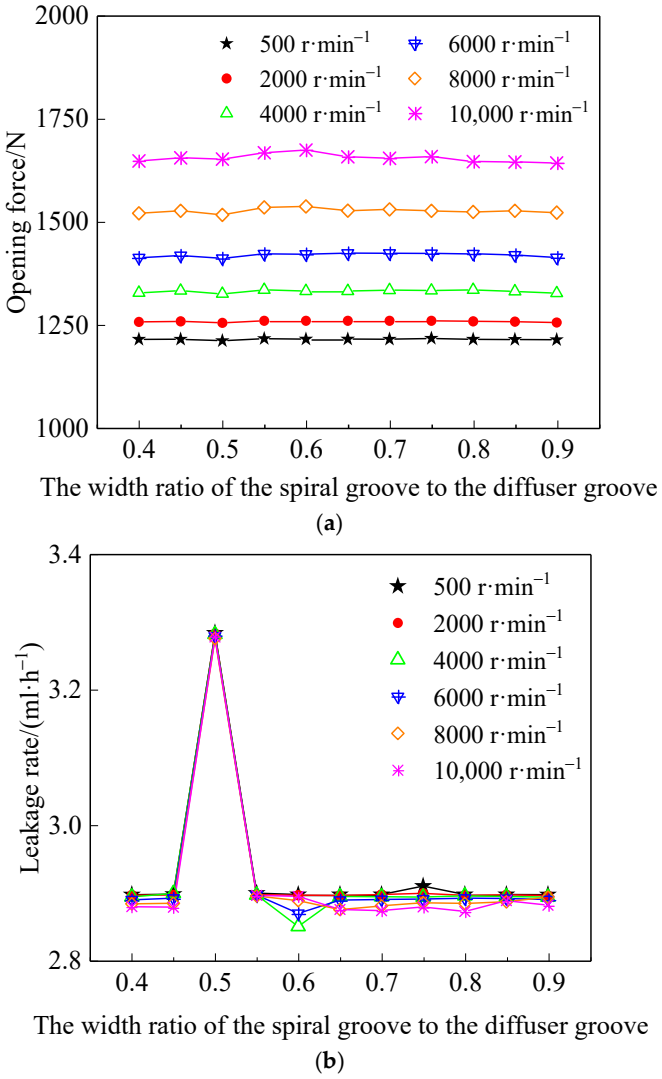


Figure 12. Influence of the width ratio of the spiral groove to the diffuser groove on the sealing performance: (**a**) Influence on the opening force; (**b**) Influence on the leakage rate. (r_k = 34 mm, $h_{ki} = h_g$ = 50 μm, r_o = 30.6 mm, N_g = 22, λ = 0.9, α = 30°, Δp = 0.5 MPa).

For the constant outer radius, the decrease in the ratio means that the spiral groove width will decrease and the diffuser groove width will increase. The distance of the fluid flowing through the working surface of the spiral groove will shorten and the obtained kinetic energy and dynamic pressure will both be reduced. However, increasing the diffuser groove width will cause the fluid to decelerate and diffuse fully. Thus, the opening force decreases insignificantly with the support of the large area of the diffuser groove.

The increase in the ratio implies that, when the outer radius remains constant, the spiral groove length increases, improving its ability to pressurize and accelerate the fluid, decreasing the pressure at the root of the spiral groove. At the same time, the spiral groove width increases, and the fluid accelerated by the spiral groove is continuously decelerated and pressurized in the spiral groove with the increasing cross-sectional area, thus increasing the hydraulic head. The increase in the hydraulic head drives the pressure at the root of the spiral groove upwards, resulting in the pressure difference on both sides of the sealing dam and leakage rate practically remains constant. When the ratio is γ = 0.5, the pressure difference on both sides of the sealing dam reaches the maximum, causing the maximum leakage rate. This might be due to the superposition of the fluid pressurization and acceleration in the spiral groove combined with sufficient deceleration and pressure diffusion in the diffuser groove.

4.3.5. Influence of the Groove Number

Figure 13a,b shows the influence of the change in groove number on the sealing performance. The sealing interface opening force slightly increases with the groove number, and the largest leakage rate is obtained for the groove number of 32. When the groove number increases, the fluid flows in the groove in an orderly manner, and the circulating flow decreases. Such behavior is beneficial to the acceleration and pressurization of the fluid within the spiral groove. However, the pressurized space of the fluid accumulated in the diffuser groove is relatively small and the deceleration and pressurization amplitude are not significant. Moreover, the cross-sectional area of a single spiral groove is reduced, strengthening the influence of the boundary layer [14]. The pumping efficiency will drop, resulting in a slow downward pressure energy trend. The trend is comprehensively reflected in the opening force, which slightly increases with the groove number. Similar to the leakage rate, the opening force reaches the maximum for the groove number of 32. As the groove number is further increased, the amplitude of deceleration and pressurization become smaller than that of the boundary layer, decreasing the opening force.

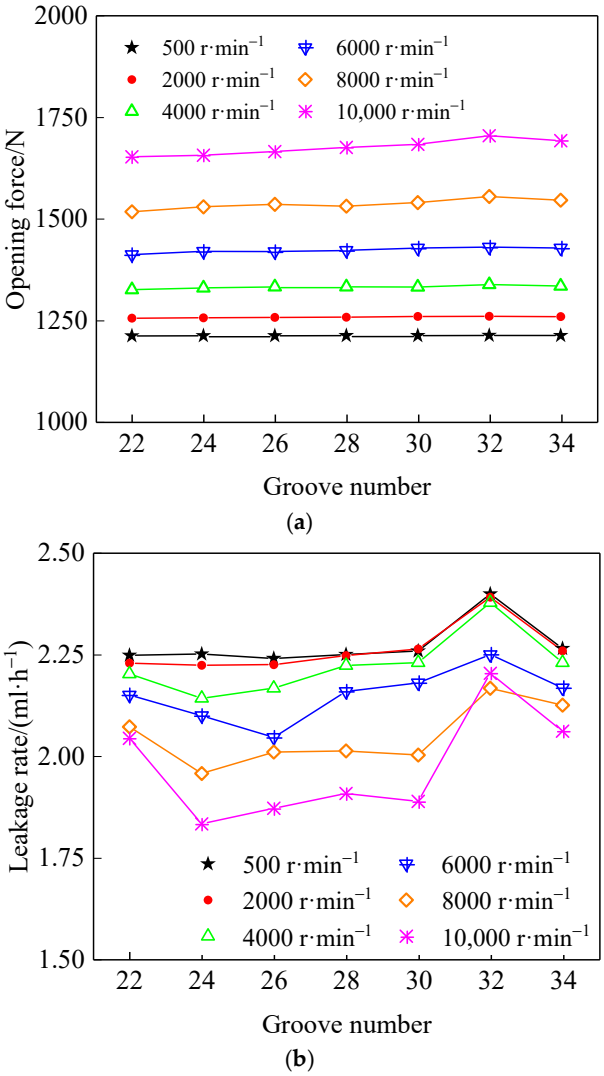


Figure 13. Influence of the groove number on the sealing performance: (**a**) Influence on the opening force; (**b**) Influence on the leakage rate. (r_k = 34 mm, h_{ki} = h_g = 50 μm, r_o = 30.6 mm, γ = 0.5, λ = 0.9, α = 30°, Δp = 0.5 MPa).

Correspondingly, when the opening force is the largest, the pressure at the root of the spiral groove also reaches its maximum, resulting in the highest sealing interface leakage

rate. With the increase in the groove number, the influence of the fluid flow boundary layer increases and the pressure at the root of the spiral groove drops, forming a relatively gentle leakage rate change.

4.3.6. Influence of Helix Angle

Considering that the fluid pumping process of the diffuser groove self-pumping hydrodynamic mechanical seal is similar to that of a centrifugal pump, the influence of the helix angle on the sealing performance is discussed. This is done by referring to the installation angle range of the centrifugal pump impeller outlet. Usually, the impeller outlet angle ranges between 22° and 50° [29]. The centrifugal pump has a wide stable working range and high efficiency. Therefore, the influence of the helix angle (ranging between 22° and 50°) on the sealing performance of the self-pumping hydrodynamic mechanical seal with CCDG is discussed.

Figure 14a,b, respectively, shows the effect of the helix angle on the sealing performance of the proposed seal. As the helix angle increases, the sealing interface opening force firstly fluctuates and attenuates before stabilizing. In this changing trend, two peaks of the sealing interface opening force are observed—the maximum values are reached for the helix angles of 26° and 34°.

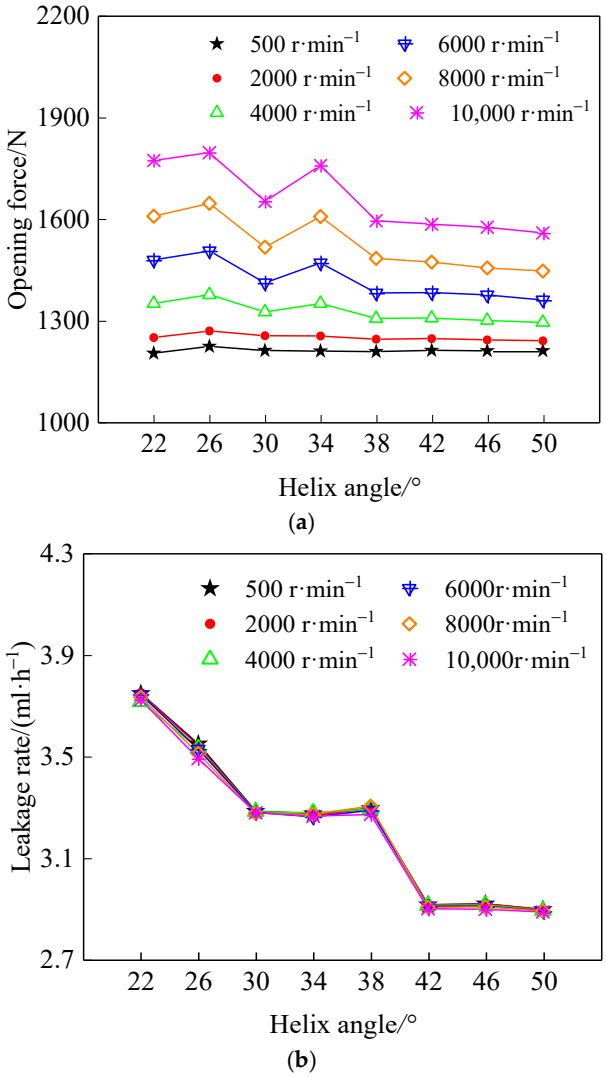


Figure 14. Influence of the helix angle on the sealing performance: (**a**) Influence on the opening force; (**b**) Influence on the leakage rate. (r_k = 34 mm, h_{ki} = h_g = 50 μm, r_o = 30.6 mm, γ = 0.5, N_g = 22, λ = 0.9, Δp = 0.5 MPa).

When the helix angle is small, its increase leads to a significant increase in the spiral groove diffusion degree. The flow is easy to separate, and the entropy area and strength increases with the spiral groove increase. Further, the flow field distortion increases, dissipating the pressure energy [30]. Next, the increase in the helix angle shortens the spiral groove length and the work stroke of the fluid in the spiral groove shortens. As a result, the peak pressure and the area of the high-pressure fluid decrease, reducing the sealing interface opening force. As illustrated in Figure 14, the opening force and leakage rate curves follow a downward trend.

With the increase in the helix angle, the spiral groove flow path becomes straighter. Although the high-pressure cloud formed by the work done by the convex side of the spiral groove gradually shrinks to the groove root, a relatively straight flow path improves the sealing medium circulation. This results in a slight decrease in the pressure difference on both sides of the sealing dam; the leakage rate shows a step-by-step decay trend.

4.4. Influence of the Operating Parameters on the Sealing Performance

The optimum structural parameters are used to analyze the influence of operating parameters on the sealing performance. The following parameters are taken as constants during the simulation: r_k = 35 mm, h_{ki} = h_g = 40 μm (or 50 μm); r_o = 30.6 mm, γ = 0.6, α = 34°, N_g = 32, and λ = 0.9.

The influence of the pressure difference between inside and outside the sealing chamber on the sealing performance is shown in Figure 15. As illustrated in Figure 15a, the increase in the sealing medium pressure difference increases the fluid pressure at the root of the spiral groove. On one hand, the sealing interface opening force at a certain rotating speed increases linearly under the combined action of the fluid acceleration and pressurization by the spiral groove and the deceleration and diffusion of the diffuser groove. On the other hand, the pressure difference on both sides of the sealing dam is increased, resulting in a linear increase in the leakage rate with the pressure difference, as shown in Figure 15b.

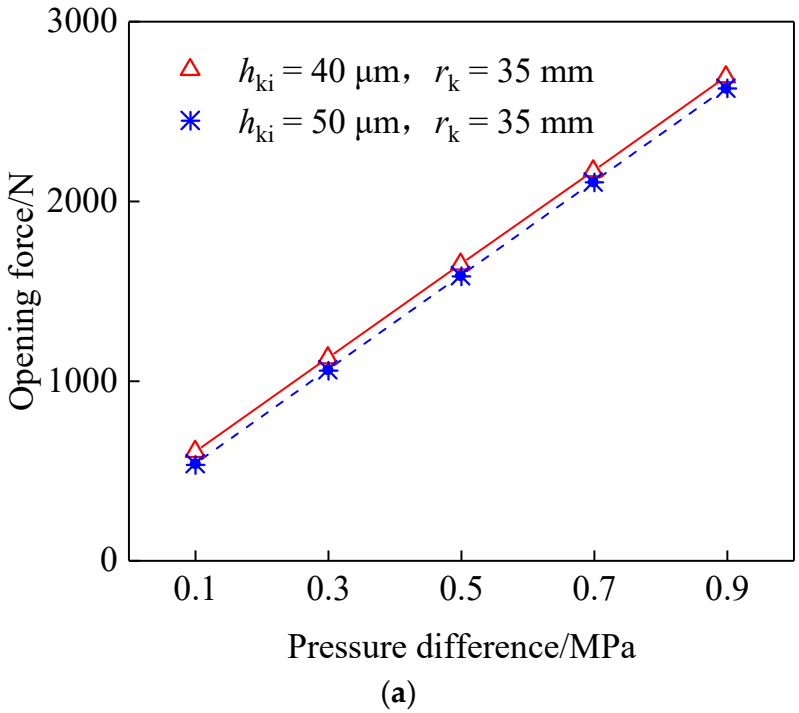


Figure 15. *Cont.*

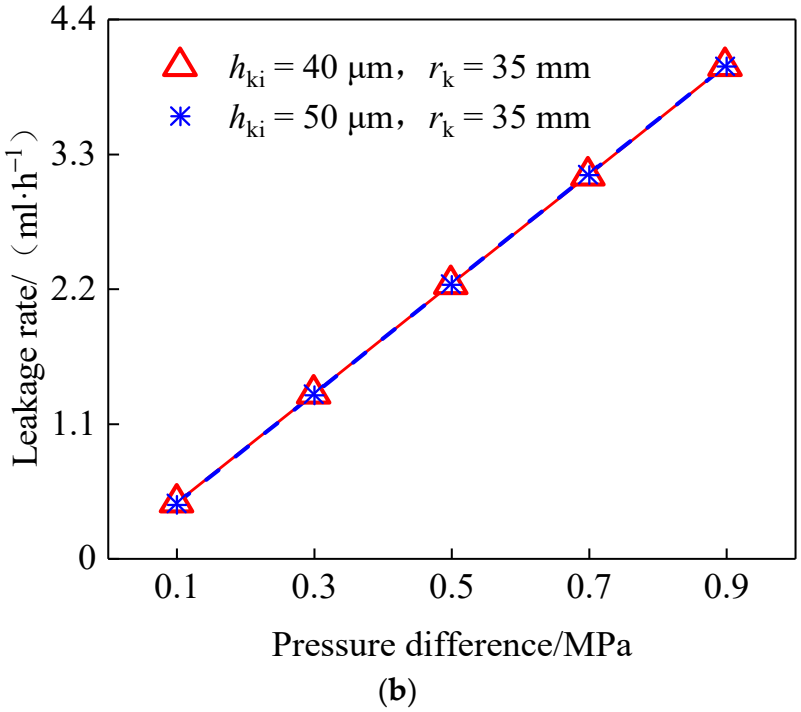


Figure 15. Influence of the sealing medium pressure difference on the sealing performance: (**a**) Influence on the opening force. (**b**) Influence on the leakage rate. (h_{ki} = h_g = 50 μm, r_o = 30.6 mm, γ = 0.6, N_g = 32, α = 34°, λ = 0.9, n = 6000 r·min^{-1}).

Figure 16 illustrates the influence of rotating speed on the sealing performance. With the increase in rotating speed, the acceleration and pressurization of the spiral groove to the fluid intensify, resulting in further deceleration and diffusion when the fluid flows through the diffuser groove. Moreover, as the rotating speed increases, the fluid pressure peak increases, linearly increasing the opening force, as shown in Figure 16. Meanwhile, increasing the rotating speed also increases the spiral groove pumping capacity, which reduces the fluid pressure at the root of the spiral groove. This results in a decrease in the pressure difference on both sides of the sealing dam, reducing the leakage rate, as shown in Figure 16.

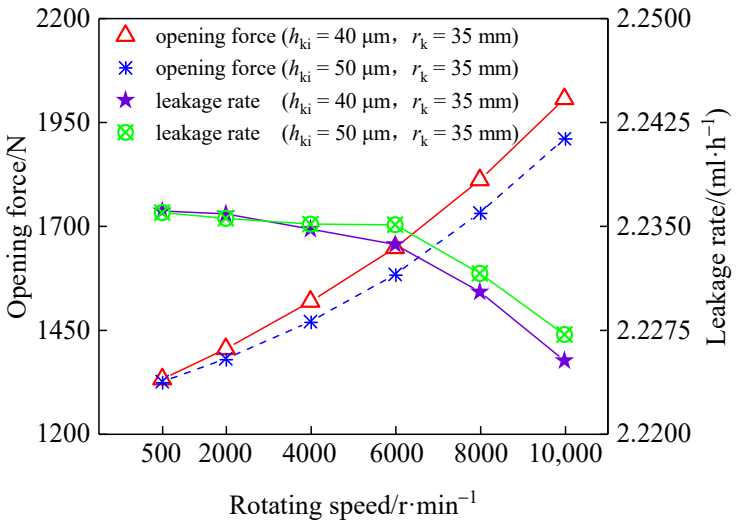


Figure 16. Influence of the rotating speed on the sealing performance. (h_{ki} = h_g= 50 μm, r_o = 30.6 mm, γ = 0.6, N_g = 32, α =3 4°, λ = 0.9, Δp = 0.5 MPa).

4.5. Working Mechanism

As shown in the analysis above, unlike in the dry gas seals and the upstream pumping mechanical seals, the self-pumping hydrodynamic mechanical seal with the CCDG operates based on the principle of the diffusor of the centrifugal pump or compressor. This approach is also different from ordinary self-pumping hydrodynamic self-pumping mechanical seals. When the proposed seal is operating, the fluid at the root of the spiral groove is driven by the working surface of the spiral groove to receive work and obtain pressure and kinetic energies. Under the centrifugal force action, the fluid in the spiral groove flows from its root to the outer diameter of the rotating ring, flowing along the convex surface contour. The fluid pumped to the diffuser groove for diffusion returns to the seal chamber.

In the process of fluid flowing from the spiral groove root to the outer diameter side of the rotating ring, it is pressurized and accelerated by the convex surface of the spiral groove. With the increase in spiral groove cross-sectional area, a share of the kinetic energy is converted into pressure energy. After the fluid flows into the diffuser groove, the velocity deceleration and pressure diffusion become sufficient due to the increase in the flow path cross-sectional area and the excellent encapsulation. Thus, more fluid kinetic energy is converted into pressure energy. Thereby, the opening force separating the rotating and the stationary rings is formed.

The fluid at the root of the spiral groove flows out, forming a low-pressure area. On the one hand, the medium pressure difference on both sides of the sealing dam decreases, and the medium can be sealed effectively. On the other hand, the fluid in the sealing chamber enters the annular groove flowing under the pressure difference through the deflector hole on the stationary ring. Then, it re-enters the root of the spiral groove and is accelerated by the convex surface of the spiral groove, increasing its speed and pressure. Under the centrifugal force action, the fluid flows to the outer diameter side of the rotating ring along the convex surface of the spiral groove and enters the sealing chamber through the diffuser groove. Thus, the self-pumping cycle forms via fluid circulation.

5. Conclusions

1. A self-pumping hydrodynamic mechanical seal with a conical convergent diffuser groove is proposed. Unlike the self-pumping hydrodynamic mechanical seal with a flat-bottomed equal cross-sectional diffuser groove, the conical convergent diffuser groove has good wrapping properties. This reduces the overflow and dilution of the high-pressure fluid in the diffuser cavity. Further, the high-pressure fluid at the sealing interface has a higher peak value and a larger area, effectively increasing the sealing interface opening force.
2. The influence of structural and operating parameters on the sealing performance of the proposed mechanical seal with a conical convergent diffuser groove is studied through numerical simulations. When the taper degree increases, the wrapping property of the diffuser cavity improves, as well as its ability to gather fluid energy. This resulted in a higher opening force. The increase in the rotating speed increases the fluid velocity and more energy accumulated in the fluid within the diffuser chamber. Therefore, a higher opening force is obtained through fluid deceleration and diffusion. The change in taper degree causes a slight change in the pressure at the root of the spiral groove, causing the pressure difference on both sides of the sealing dam to fluctuate, resulting in fluctuations in the seal leakage rate. For the same taper degree, the increased rotating speed also increases the fluid flow and decreases the pressure at the root of the spiral groove, thereby reducing the pressure difference on both sides of the sealing dam and the leakage rate.
3. Regarding the actual sealing performance of the self-pumping hydrodynamic mechanical seal with a conical convergent diffuser groove, the authors aim to conduct experimental verification in subsequent research.

Author Contributions: The study conception and design, J.S., C.M., Q.Y. and X.S.; Conceptualization, J.S.; Formal analysis, C.M.; Funding acquisition, J.S.; Investigation, Q.Y.; Software, X.S.; Writing—original draft, X.S. All authors have read and agreed to the published version of the manuscript.

Funding: This research was funded by National Natural Science Foundation of China, grant number 52075268, the Key R&D Program of Jiangsu Province, grant number BE2021062, and the Key R&D Industrialization Projects of Zhangjiagang, grant number ZKZ2006.

Institutional Review Board Statement: Not applicable.

Informed Consent Statement: Not applicable.

Data Availability Statement: Data is contained within the article.

Conflicts of Interest: The authors declare no conflict of interest.

References

1. Alan, O.L. *Principles and Design of Mechanical Face Seals*; China Machine Press: Beijing, China, 2016.
2. Lai, T. Development of non-contacting, non-leaking spiral groove liquid face seals. *Lubr. Eng.* **1994**, *50*, 625–631.
3. Du, Q. Effects of grooved ring rotation and working fluid on the performance of dry gas seal. *Int. J. Heat Mass Transf.* **2018**, *126*, 1323–1332. [CrossRef]
4. Wang, Y.M.; Liu, W.; Liu, Y. Current research and developing trends on non-contacting mechanical seals. *Hydraul. Pneum. Seals* **2011**, *31*, 29–33.
5. Meng, X.; Tu, Z.; Ma, Y.; Jiang, J.; Peng, X. Topology optimization of liquid lubricating zero-leakage mechanical face seals. *Tribol. Int.* **2022**, *169*, 107490. [CrossRef]
6. Shen, C.; Khonsari, M.M. Numerical optimization of texture shape for parallel surfaces under unidirectional and bidirectional sliding. *Tribol. Int.* **2015**, *82 Pt A*, 1–11. [CrossRef]
7. Chen, H.L.; Gui, K.; Zhao, B.J.; Chen, M.M.; Ren, K.T.; Liu, J.F. Research on Multi-objective and Multi-condition Optimization of Upstream Pumping Mechanical Seal. *Lubr. Eng.* **2020**, *45*, 19–25.
8. Yan, R.; Chen, H.; Zhang, W.; Hong, X.; Bao, X.; Ding, X. Calculation and verification of flow field in supercritical carbon dioxide dry gas seal based on turbulent adiabatic flow model. *Tribol. Int.* **2022**, *165*, 107275. [CrossRef]
9. Gani, M.; Santos, I.F.; Arghir, M.; Grann, H. Model validation of mechanical face seals in two-phase flow conditions. *Tribol. Int.* **2022**, *167*, 107417. [CrossRef]
10. Brunetière, N.; Rouillon, M. Fluid flow regime transition in water lubricated spiral grooved face seals. *Tribol. Int.* **2021**, *153*, 106605. [CrossRef]
11. Pan, X.D.; Guo, W.; Cui, J. Exploration and optimized application of mechanical seal aided flushing system. *Petro Chem. Equip.* **2019**, *22*, 106–108.
12. Qiu, Y.; Khonsari, M.M. Thermohydrodynamic analysis of spiral groove mechanical face seal for liquid applications. *J. Tribol.* **2012**, *134*, 021703. [CrossRef]
13. Chen, H.; Zuo, M.; Wu, Q.; Xu, C.; Wang, Y.; Li, S. Solid-liquid two-phase flow characteristics of lubricating film in upstream pumping mechanical seal. *J. Drain. Irrig. Mach. Eng.* **2015**, *33*, 685–690.
14. Sun, J.J.; Wang, M.; Zhou, M.; Tu, Q.A.; Hai, L.M.; Li, Z.H.; Li, Z.X.; Wang, X.; Wang, Y. Self-Pumping Mechanical Seal Based on Fluid Dynamic Pressure Principle. CN Patent 103267132A, 28 May 2013.
15. Zhou, M.; Sun, J.; Ma, C.; Yu, Q.; Zhou, P. Analysis of self-pumped hydrodynamic mechanical seal performance. *CIESC J.* **2015**, *66*, 687–694.
16. Lu, J.; Sun, J.; Chen, W. Performance comparison of self-pumping and spiral groove mechanical seals. *CIESC J.* **2016**, *67*, 4370–4377.
17. Gu, D.; Sun, J.; Ma, C. Orthogonal test of self-pumping mechanical seal based on numerical simulation. *CIESC J.* **2015**, *66*, 2464–2473.
18. Chen, Q.; Sun, J. Analysis of self-cleaning for self-pumping hydrodynamic and hydrostatic mechanical seal. *Tribology* **2019**, *39*, 259–268.
19. Sun, J.; Ma, C.; Yu, Q.; Lu, J.; Zhou, M.; Zhou, P. Numerical analysis on a new pump-out hydrodynamic mechanical seal. *Tribol. Int.* **2017**, *106*, 62–70.
20. Ge, C.; Sun, J.; Su, X.; Ma, C.; Yu, Q. Performance analysis on diffuser self-pumping hydrodynamic and hydrostatic mechanical seal. *CIESC J.* **2020**, *71*, 2202–2214.
21. Nau, B.S. An historical review of studies of polymeric seals in reciprocating hydraulic systems. *Proc. Inst. Mech. Eng. Part J J. Eng. Tribol.* **1999**, *213*, 215–226. [CrossRef]
22. Li, Y.; Song, P.Y.; Xu, H.J. Performance analyses of the spiral groove dry gas seal with inner annular groove. *Appl. Mech. Mater.* **2013**, *420*, 51–55. [CrossRef]
23. Bo, R. Finite Element Analysis of the Spiral Groove Gas Face Seal at the Slow Speed and the Low Pressure Conditions—Slip Flow Consideration. *Tribol. Trans.* **2000**, *43*, 411–418. [CrossRef]

24. Ma, C. Study on the Lubrication Computational Model and Antifriction Performance of Textured Surfaces. Ph.D. Thesis, China University of Mining and Technology, Xuzhou, China, 2010.
25. Hu, X.P.; Song, P.Y. Theoretic Analysis of the Effect of Real Gas on the Performance of the T-Groove and Radial Groove Dry Gas Seal. *Appl. Mech. Mater.* **2013**, *271*, 1218–1223. [CrossRef]
26. Yang, W.; Hao, M.; Cao, H.; Yuan, J.; Li, H. Analysis of cavitation of downstream pumping spiral groove liquid film seal considering mass conserving boundary condition. *CIESC J.* **2018**, *69*, 3932–3943.
27. Zhang, J.; Chen, Q.; Shi, M.; Zhou, H.; Xu, L. Interaction and influence of a flow field and particleboard particles in an airflow forming machine with a coupled Euler-DPM model. *PLoS ONE* **2021**, *16*, e0253311. [CrossRef] [PubMed]
28. Hu, K.; Li, Z.B. *Detailed Explanation of ANSYS ICEM CFD Engineering Example*; Posts & Telecom Press: Beijing, China, 2014.
29. Turbine and Compressor Lab on Xi'an Jiaotong University. *Fundamentals of Centrifugal Compressor*; Machinery Industry Press: Beijing, China, 1980.
30. Jiang, P.Z. *Process Fluid Machinery*; Chemical Industry Press: Beijing, China, 2001.